Int. J. Nanosci. Nanotechnol., Vol. 15, No. 1, March. 2019, pp. 11-19

Elastic Properties and Fracture Analysis of Perfect and Boron-doped C2N-h2D Using Molecular Dynamics Simulation

Amir Ameri[1], Shahram Ajori[1,2*] and Reza Ansari[1]

[1]Department of Mechanical Engineering, Faculty of Engineering, University of Guilan, P.O.Box 3756, Rasht, Iran.
[2]Department of Mechanical Engineering, Faculty of Engineering, University of Maragheh, P.O.Box 83111-55181, Maragheh, Iran.

(*) Corresponding author: sajori@maragheh.ac.ir
(Received: 05 February 2017 and Accepted: 22 October 2018)

Abstract

This paper explores the mechanical properties and fracture analysis of C2N-h2D single-layer sheets using classical molecular dynamics (MD) simulations. Simulations are carried out based on the Tersoff potential energy function within Nose-Hoover thermostat algorithm at the constant room temperature in a canonical ensemble. The influences of boron (B) doping on the mechanical properties, i.e. Young's and bulk moduli and ultimate strength and strain of C2N-h2D single-layer sheets are studied and the effects of size and doping percentage on the aforementioned properties are explored. The results demonstrate lower strength and stiffness of C2N-h2D single-layer sheets compared to graphene. It is also demonstrated that unlike the strength of C2N-h2D single-layer sheet, the stiffness of C2N-h2D single-layer sheet is larger than that of silicene nanosheet. In addition, it is observed that doping of B atoms on C2N-h2D single-layer sheets intensely reduces the mechanical properties, whereas this reduction increases by rising the percentage of B-doping. Furthermore, the fracture process of C2N-h2D and B-doped C2N-h2D single-layer sheets is illustrated.

Keywords: *C2N-h2D, Doping, Molecular dynamics simulations, Mechanical properties, Fracture.*

1. INRODUCTION

Graphene [1], due to its extraordinary mechanical [2], thermal [3], electrical [4] and optical [5] properties, definitely is responsible for the recent improvements in the fields of nanotechnology and nanoscience. The recent scientific studies on graphene [6-10] have motivated scientists to introduce new two-dimensional structures employing the elements other than carbon [5], especially nitrogen due to its ability to form sp2 hybridization together with strong covalent bonds with carbon atoms [11-16]. Due to tunable structures and properties of N-containing 2-D structures, they have many potential applications. Recently, Mahmood et al. [17] synthesized a multifunctional new nitrogenated holey two-dimensional (C2N-h2D) layered structure with uniform holes and nitrogen atoms via simple production methods with various potential applications in electronics, sensors, and catalysis. Other than common types of defects which are inevitable in synthesizing of any nanostructures, i.e. vacancy and Stone-Wales which are comprehensively investigated [10, 18-20], substitution atom impurities are the type of defects that their effect on the mechanical properties and fracture analysis is not investigated as well as common defects. Also, most of these studies are performed on graphene and well-known nano-structures [21-28]. Accordingly, it can be observed that boron atom because of its similar size and three valance electrons is the best choice for chemical doping of carbon/nitrogen-based materials.

As C2N-h2D has been synthesized quiet recently there are few investigations which

concentrate on physiochemical properties [29-33]. So, the mechanical properties of C2N-h2D have not been investigated comprehensively, this study aims to investigate the mechanical properties and fracture analysis of C2N-h2D and B-doped C2N-h2D single-layer sheets, i.e. Young's and bulk moduli and ultimate strength and strain by implementing classical molecular dynamics (MD) simulations. Also, the effects of size and doping percentage on the aforementioned parameters are investigated.

2. METHODOLOGY AND MODEL

In this study, the MD simulations based on Tersoff potential energy function (PEF) [34,35] with optimized C-BN parameters [36] are carried out employing Large-scale Atomic/Molecular Massively Parallel Simulator (LAMMPS) [37] in order to investigate the mechanical properties and fracture analysis of C2N-h2D and B-doped C2N-h2D square single-layer sheets. In all simulations, the canonical ensemble (NVT) is applied by employing Nose-Hoover thermostat algorithm [38] to control the fluctuation of temperature, within the Velocity-Verlet integrator algorithm with time step of 1 fs to integrate the Newtonian equations of motion [39]. Conjugate gradient algorithm with an energy convergence norm is also implemented to minimize energy of simulation system in order to minimize relative energies sufficiently. After initial energy minimization, the uni- and bi-axial tensile loads are applied by imposing a displacement of 0.01 Å to the boundaries to compute the Young's and bulk moduli, respectively [40]. Schematic representations of imposing uni- and bi-axial tensile loads on C2N-h2D single-layer sheet are given in Figures 1 (b) and 1 (c), respectively. As shown in these figures, four rows of atoms (one benzene ring) in each side of sheets are held fix as boundaries. Afterwards, the system is relaxed for 10 ps. Then, the strain energy of nanosheets is computed in each step and the desired mechanical properties are calculated [40].

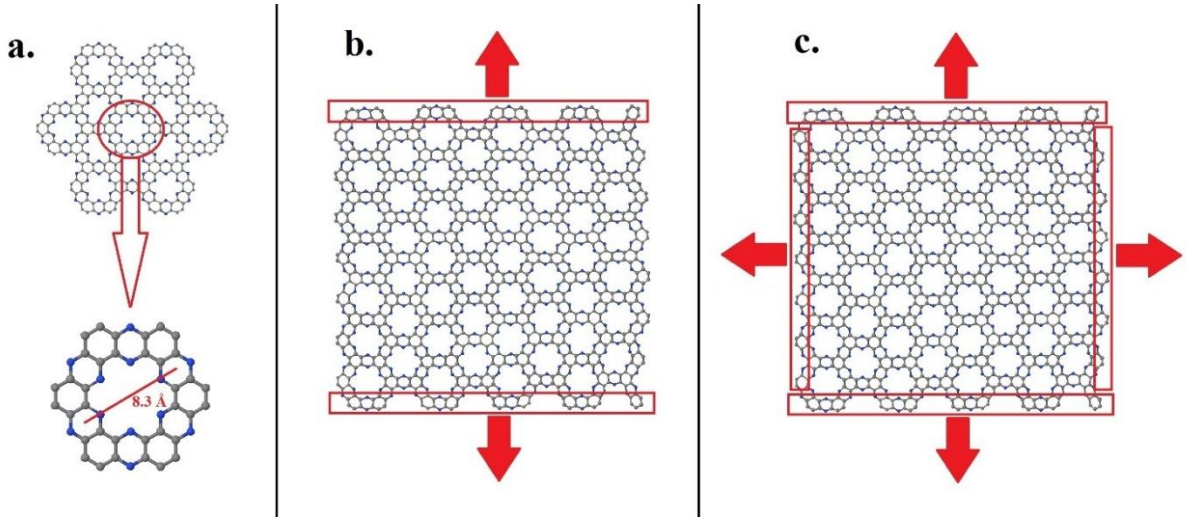

Figure 1. *Schematic representation of (a) C2N-h2D structure and dimensions of unit cell, (b) imposing uniaxial tensile load on C2N-h2D single-layer sheet and (c) imposing biaxial tensile load on C2N-h2D single-layer sheet.*

3. RESULTS AND DISCUSSION

In this section, results of MD simulations for the mechanical properties of C2N-h2D single layer sheets and B-doped C2N-h2D single-layer sheets such as Young's and bulk moduli, ultimate strength and strain are given. Side length size of square sheets of C2N-h2D varies from 40 Å to 90 Å (Figure 2.), with 518 to 2526 atoms, respectively. In order to investigate the

effect of doping, a C2N-h2D sheet with the size of 60Å×60Å and B percentage of 5%, 10%, 15%, 20%, 25%, 50% is determined.

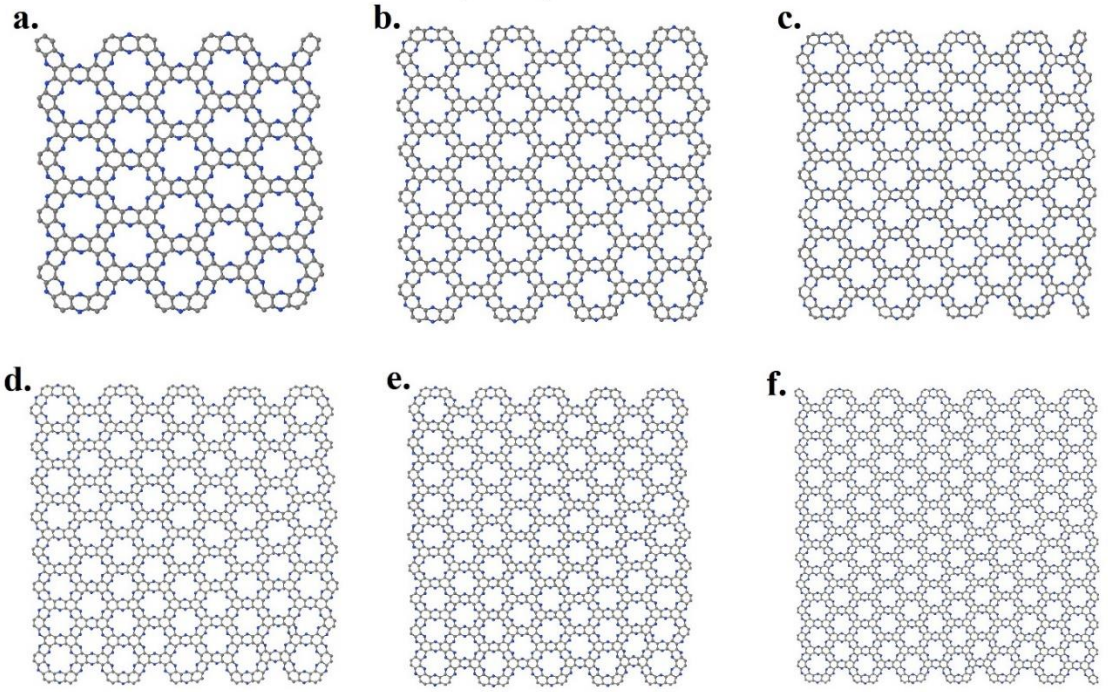

***Figure 2**. Schematic representation of size variation of C2N-h2D single-layer sheet with the side length of (a) 40 Å, (b) 50 Å, (c) 60 Å, (d) 70 Å, (e) 80 Å and (f) 90 Å.*

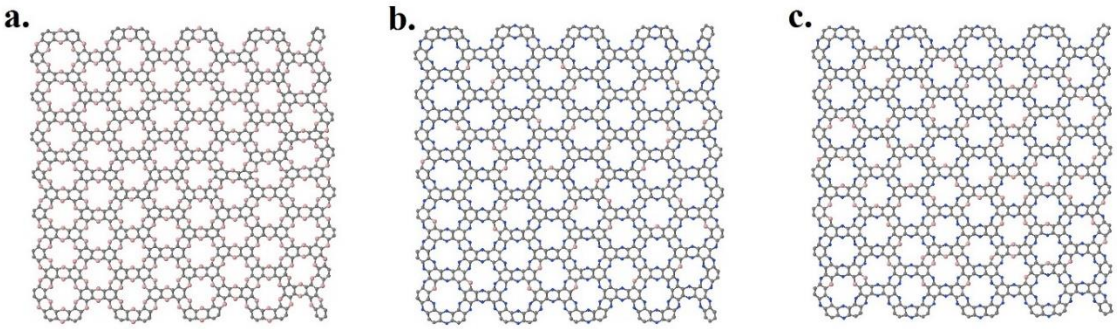

***Figure 3**. Schematic representation of (a) C2B-h2D single-layer sheet, (b) and (c) 10% and 20% of B.*

Also, a model of C2B-h2D sheet, which is formed by substituting N atoms of C2N-h2D sheet with B atoms, is simulated and compared. The schematic of 10% and 20% of B doping percentage and C2B-h2D single-layer sheet is shown in Figure 3.

3.1. Pure C2N-h2D

3.1.1 Uniaxial Tension

The MD simulation results reveal that Young's modulus of C2N-h2D square sheet with side length of 60 Å is computed around 88.6 Pa.m which can be compared with those of graphene (272 Pa.m) [10] and silicene nanosheet (68.7 Pa.m) [40]. It is observed that Young's modulus of C2N-h2D single-layer sheet is about 67% lower than that of graphene and 29% higher than that of silicene nanosheet with similar dimensions. The variation of Young's modulus with the side length of C2N-h2D square sheets is represented in Figure 4. As revealed, Young's modulus of the smallest C2N-h2D sheet is computed around 102.6 Pa.m which by a linear-like relation

reduces to 70.2 Pa.m as side length increases to 90 Å.

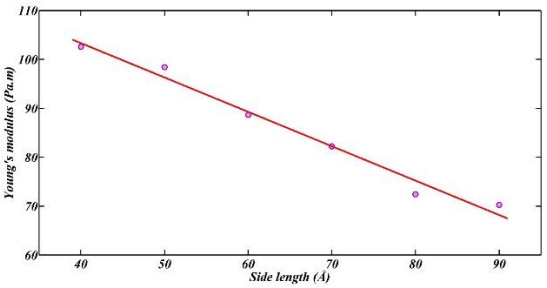

Figure 4. *Variation of Young's modulus with the length.*

Moreover, it is observed that the ultimate strength of C2N-h2D square sheet with side length of 60 Å is computed around 13.53 GPa which is about 81% lower than that of graphene [10] and 19% lower than that of silicene nanosheet [40] with similar dimension. It is further obtained from simulations that ultimate strain of C2N-h2D square sheet (9.53%) is about 58% lower than that of graphene [10] and 64% lower than that of silicene nanosheet [40] with similar dimension.

To explore the variation of ultimate stress and strain with the size of C2N-h2D square sheets, Figures 5 and 6 are illustrated, respectively. In the case of ultimate strength, it is observed that ultimate strength linearly reduces by raising the size of C2N-h2D square sheets. For example, ultimate strength of C2N-h2D square sheet with side length of 90 Å is computed about 46% lower than that of C2N-h2D square sheet with side length of 40 Å.

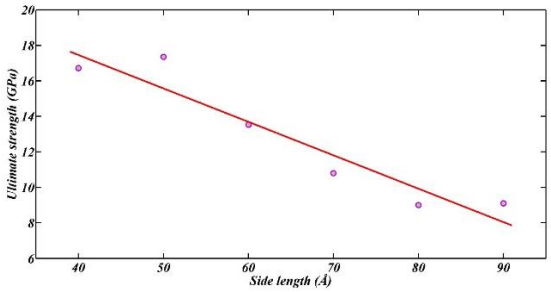

Figure 5. *Variation of ultimate strength with the length.*

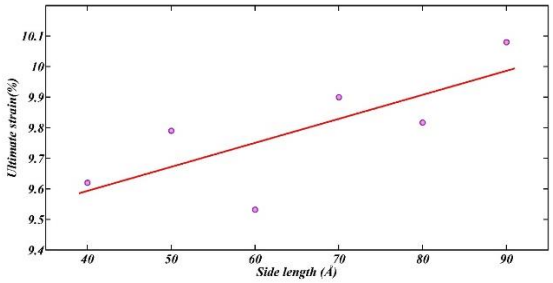

Figure 6. *Variation of ultimate strain with the length.*

It can be revealed from Figures 6 that unlike the ultimate strength, the ultimate strain smoothly increases by a linear-like relation as the size of C2N-h2D square sheets rises. For instance, the ultimate strain of 90 Å×90 Å C2N-h2D sheet is about 1.05 times bigger than that of 40 Å×40 Å C2N-h2D sheet.

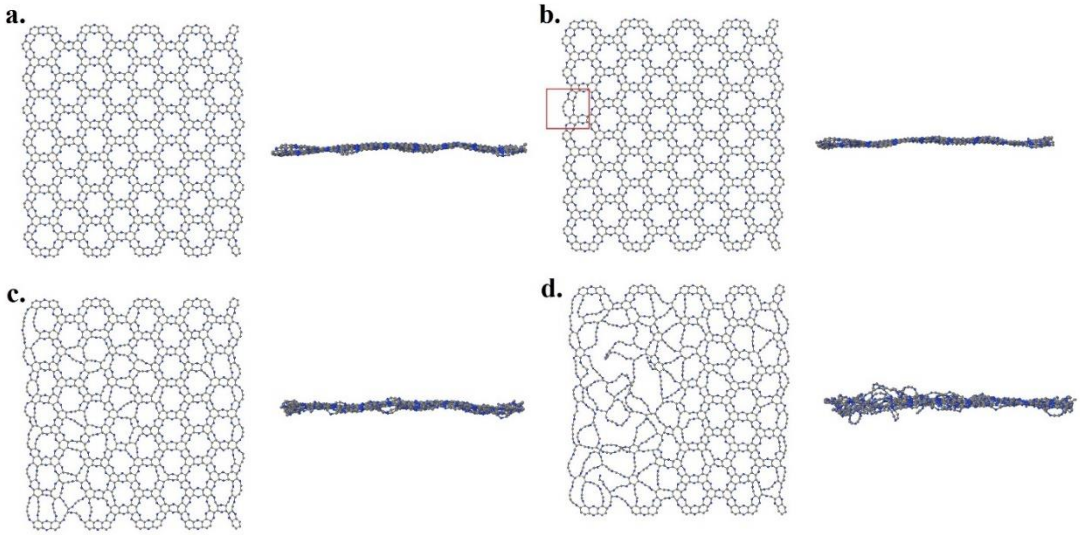

Figure 7. *Fracture process of a 60 Å×60 Å C2N-h2D single-layer sheet.*

The failure process of a 60 Å×60 Å C2N-h2D single-layer sheet is depicted in Figure 7. From this figure, it is observed that the bond breakage is initiated from the atoms located at both free sides of sheet (Figure 7(b)), and propagates vertically towards both boundaries. Simultaneously, due to bond breakage, some topological defects irregularly appear (Figure 7(c)). Further, concentration of defects mostly at the corner zone near the boundaries of both sides causes the failure of sheet. Also, the formation of atomic chains is depicted in Figure 7(d).

3.1.2 Biaxial Tension

Subsequently, to investigate bulk modulus, biaxial loads are imposed to the C2N-h2D square sheets [40]. Based on the MD simulations results, the bulk modulus of a 60 Å×60 Å C2N-h2D square sheet is computed 100 Pa.m, which is around 2 times bigger than that of silicene nanosheet with similar dimensions [40]. Also, the variation of bulk modulus with the size of C2N-h2D square sheets is illustrated in Figure 8. As shown in this figure, the bulk modulus of the smallest C2N-h2D sheet with 40 Å side length is computed around 112.7 Pa.m which based on a linear-like relation reduces to 75 Pa.m as side length increases to 90 Å.

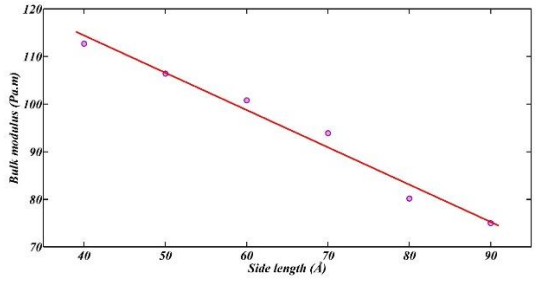

Figure 8. *Variation of bulk modulus with the length.*

3.2 B-Doped C2N-h2D Single-Layer Sheet

As mentioned previously, a 60 Å×60 Å C2N-h2D single-layer sheet is selected for B doping with atomic percentages of 5%, 10%, 15%, 20%, 25% and 50%. The B atoms are doped instead of N atoms. Then, the mechanical properties and fracture progress of mentioned B-doped C2N-h2D single-layer sheets and C2B-h2D single-layer sheet are calculated.

3.2.1 Uniaxial Tension

In order to study the mechanical behavior of C2N-h2D, samples for the stress-strain graph for pure and doped structures are presented in Figure 9. Accordingly, Young's modulus of pure C2N-h2D square sheet with side length of 60 Å, which is selected for doping of B atoms, is calculated around 88.6 Pa.m. As N atoms are fully substituted by B atoms, Young's modulus is calculated around 71.4 Pa.m which is approximately 19% lower than that of similar pure C2N-h2D square sheet.

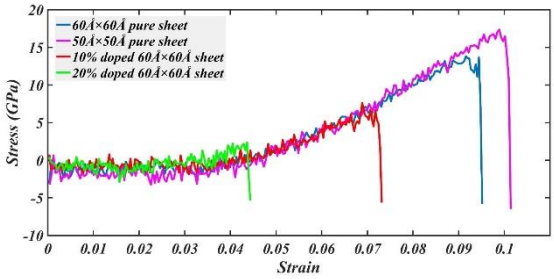

Figure 9. *Stress-strain graph for pure and doped structures.*

In order to identify the effect of percentage of B doping on Young's modulus of C2N-h2D square sheets, Figure 10 is given. As shown in this figure, B-doping reduces Young's modulus of C2N-h2D single-layer sheets. The lowest and highest reductions are obtained around 14% and 49% which occur in 5% and 50%, respectively.

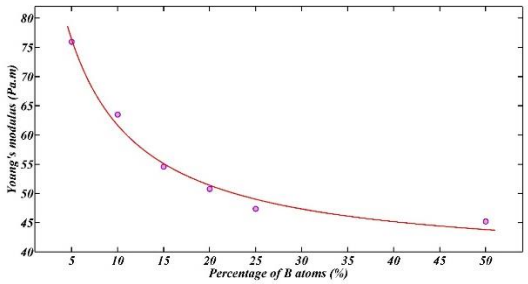

Figure 10. *Variation of Young's modulus with the percentage of B atoms.*

It is also observed that Young's modulus of B doped sheets decreases by a homographic-like relation as percentage of B atoms on the sheet increases. For example, Young's modulus of sheet with 25% of percentage of B atoms is about 29% lower than that of sheet with 5% of B atoms doped on C2N-h2D square sheet.

The MD simulation results reveal that the ultimate strength and strain of C2B-h2D square sheet are 13.4 GPa and 12.49%, correspondingly. Comparing them with the ultimate strength and strain of C2N-h2D square sheet with side length of 60 Å, reveals that by replacing of all N atoms with B atoms ultimate strength reduces around 1% and the ultimate strain increases around 31%. Furthermore, the variation of ultimate stress and strain of 60 Å×60 Å C2N-h2D sheet with the different atomic percentage of B atoms are computed and illustrated in Figures 11 and 12, correspondingly.

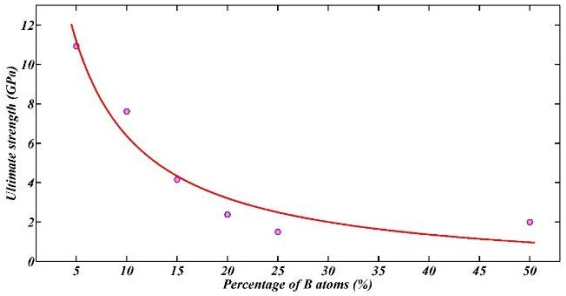

Figure 11. *Variation of ultimate strength with the percentage of B atoms.*

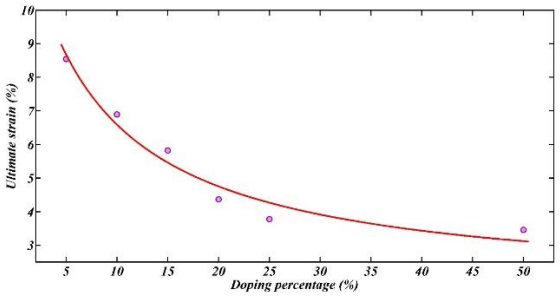

Figure 12. *Variation of ultimate strain with the percentage of B atoms.*

From these figures, it is observed that B-doping reduces both the ultimate strength and strain. The highest reduction of the ultimate strength and strain is around 89% and 64% which occur at 25% and 50%, respectively. Further, it is observed that the ultimate strength and strain of B-doped sheets reduce by rising of the percentage of B atoms. For example, the ultimate strength and strain of the sheet with 25% of B atoms, respectively are computed 86% and 56% lower than those of the sheet with 5% of B atoms.

Making a comparison between the similar doping percentage (~4%) of boron atom on C2N-h2D and graphene [27] demonstrates that the mechanical properties of C2N-h2D is more sensitive to doping than graphene. For example, the reduction in the stiffness and strength of C2N-h2D (~14 and ~19%, respectively) is higher than those of graphene, correspondingly, i.e. ~5% and ~8%.

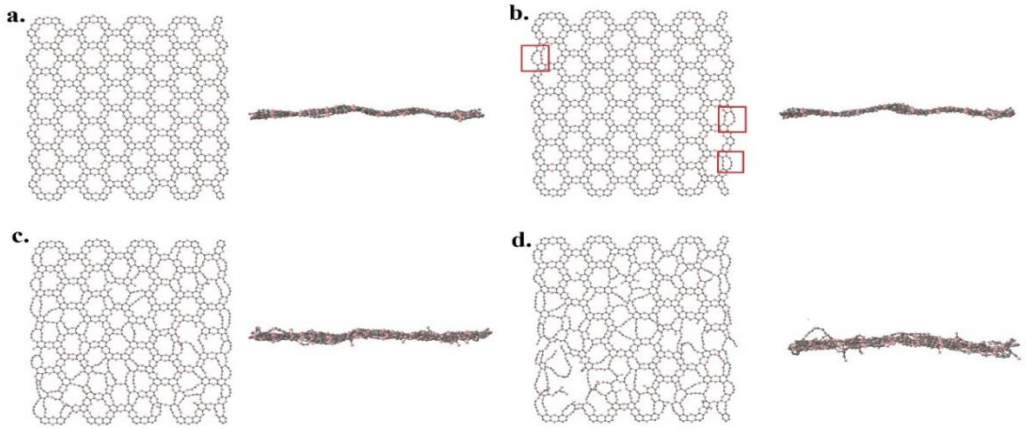

Figure 13. *Fracture process of a 60Å×60Å C2B-h2D single-layer sheet.*

.

Furthermore, the fracture process of C2B-h2D with 10% of B atoms is illustrated in Figures 13 and 14, respectively. Similar to pure C2N-h2D

sheet, initiation of fracture occurs with breakage of bonds of side atoms. Unlike pure C2N-h2D (Figure 7) sheet and C2B-h2D (Figure 13), appearance of topological defects and formation of new atomic chains in B-doped C2N-h2D sheet (Figure 14) are also observed.

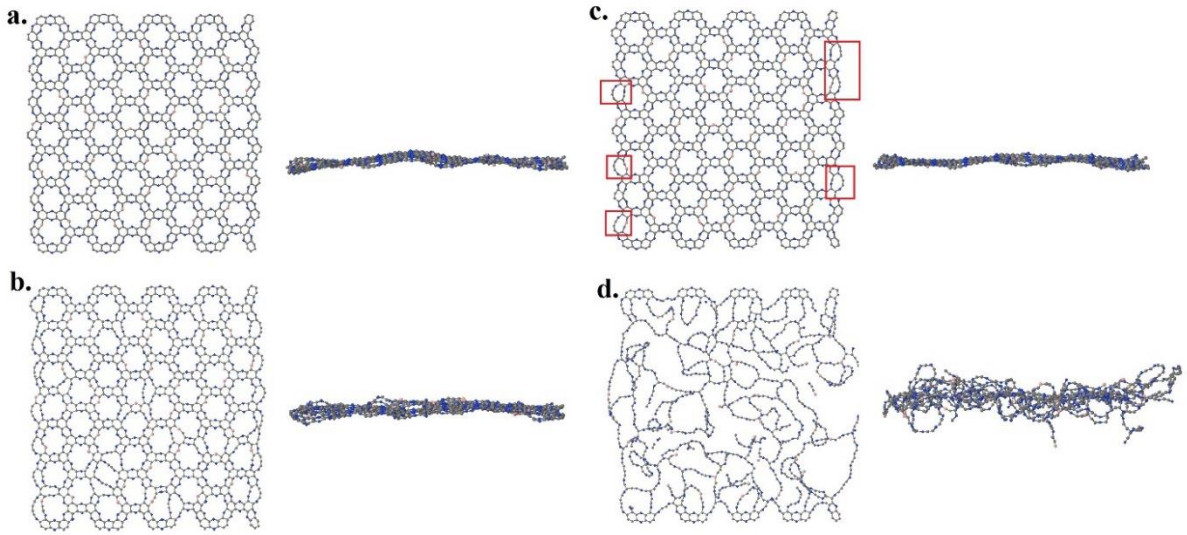

Figure 14. *Fracture process of 10% of percentage B-doped C2N-h2D single-layer sheet.*

3.2.2 Biaxial Tension

The bulk modulus of C2B-h2D square sheet is computed about 126.6 Pa.m which is approximately 1.26 bigger than that of C2N-h2D square sheet (100 Pa.m). As shown in Figure 15, which illustrates the variation of the bulk modulus with the percentage of B atoms, the bulk modulus of B-doped C2N-h2D single-layer sheet is larger than that of C2N-h2D pure sheet and homographically reduces by rising the percentage of B atoms. For example, the discrepancy between the bulk modulus of B-doped C2N-h2D single-layer sheet with 5% and 25% of B atom is around 7.7%.

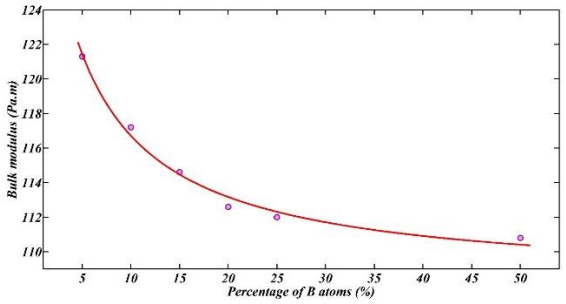

Figure 15. *Variation of bulk modulus with the percentage of B atoms.*

4. CONCLUSION

In this study, MD simulations based on Tersoff potential energy function within the canonical ensemble (NVT) were utilized in order to investigate the mechanical properties and fracture analysis of C2N-h2D and B-doped C2N-h2D square sheets. The results demonstrated that the ultimate strength and strain of C2N-h2D square sheet are significantly lower than those of graphene and silecene nanosheet. Also, Young's modulus of C2N-h2D square sheet is lower and higher than those of graphene and silicone, respectively. Moreover, it was demonstrated that unlike the ultimate strain, the Young's and bulk moduli and the ultimate strength of C2N-h2D square sheets decrease by increasing the size of sheets. Additionally, the results showed that the doping of C2N-h2D square sheets with B atoms instead of N atoms reduces mechanical properties of sheet, and this reduction increases as the percentage of B-doping increases. Finally, fracture processes of C2N-h2D and of B-doped C2N-h2D square sheets were illustrated and the formation of topological defects and atomic chains were depicted.

REFERENCES

1. Novoselov, K. S., Geim, A. K., Morozov, S. V., Jiang, D., Zhang, Y., Dubonos, S. V., Grigorieva, I. V., Firsov, A., (2004). "Electric field effect in atomically thin carbon films", *Science*, 306: 666–669.
2. Lee, C., Wei, X., Kysar, J. W., Hone, J., (2004). "Measurement of elastic properties and instricnt strength of monolayer graphene", *Science*, 306: 385-388.
3. Balandin, A. A., Ghosh, S., Bao, W., Calizo, I., Teweldebrhan, D., Miao, F., Lau, C. N., (2008). "Superior thermal conductivity of single-layer graphene ", *Nano Lett.*, 8: 902-907.
4. Neto, A. H. C., Guinea, F., Peres, N. M., Novoselov, K. S., Geim, A. K., (2009). "The electronic properties of graphene", *Rev. Mod. Phys.*, 81: 109-162.
5. Grigorenko, A. N., Polini, M., Novoselov, K. S., (2012). "Graphene plasmonics", *Nature Photonics*, 6: 749-758.
6. Zhang, Y., Tan, Y. W., Stormer, H. L., Kim, P., (2005). "Experimental observation of the quantum Hall effect and Berry's phase in graphene", *Nature*, 438: 201-204.
7. Novoselov, K. S., Geim, A. K, Morozov, S. V., Jiang, D., Katasnelson, M. I., Grigorieva, I. V., Dubonos, S. V., Firsov, A. A., (2005). "Two-dimensional gas of massless Dirac fermions in graphene", *Nature*, 438: 197-200.
8. Azamat, J., (2018). "Application of Functionalized Graphene Oxide Nanosheet in Gas Separation", *International Journal of Nanoscience and Nanotechnology*, 14(2): 165-175.
9. Topsakal, M., Cahangirov, S., Ciraci, S., (2010). "The response of mechanical and electronic properties of graphane to the elastic strain", *Appl. Phys. Lett.*, 96: 091912.
10. Ansari, R., Ajori, S., Motevalli, B., (2012). "Mechanical properties of defective single-layered graphene sheets via molecular dynamics simulation", *Superlattices Microstruct.*, 51: 274-289.
11. Mas-Balleste, R., Gomez-Navarro, C., Gomez-Herrero, J., Zamora, F., (2011). "2D materials: to graphene and beyond", *Nanoscale*, 3: 20-30.
12. Wang, X., Li, X., Zhang, L., Yoon, Y., Weber, P. K., Wang, H., Guo, J., Dai, H., (2009). "N-doping of graphene through electrothermal reactions with ammonia", *Science*, 324: 768-771.
13. Wei, D., Liu, Y., Wang, Y., Zhang, H., Huang, L., Yu, G., (2009). "Synthesis of N-Doped Graphene by Chemical Vapor Deposition and Its Electrical Properties", *Nano lett.*, 9: 1752-1758.
14. Qu, L., Liu, Y., Baek, J. B., Dai, L., (2010). "Nitrogen-doped graphene as efficient metal-free electrocatalyst for oxygen reduction in fuel cells", *ACS Nano*, 4: 1321-1326.
15. Wang, H., Zhang, C., Liu, Z., Wang, L., Han, P., Xu, H., Zhang, K., Dong, S., Yao, J., Cui, G., (2011). "Nitrogen-doped graphene nanosheets with excellent lithium storage properties", *J. Mater. Chem.*, 21: 5430-5434.
16. Gutzler, R., erepichka, D. F., (2013). "π-Electron Conjugation in Two Dimensions", *J. Am. Chem. Soc.*, 135: 16585-16594.
17. Mahmood, J., Lee, E. K., Jung, M., Shin, D., Jeon, I. Y., Jung, S. M., Choi, H. J., Seo, J. M., Bae, S. Y., Sohn, S. D., Park, N., Oh, J. H, Shin, H. J., Baek, J. B, (2015). "Nitrogenated holey two-dimensional structures", *Nat. Commun.*, 6: 6486.
18. Xiao, J. R. , Staniszewski, J., Gillespie, J. W., (2009). "Fracture and progressive failure of defective graphene sheets and carbon nanotubes", *Compos. Struct.*, 88: 602-609.
19. Xiao, J. R. , Staniszewski, J., Gillespie, J. W., (2010). "Tensile behaviors of graphene sheets and carbon nanotubes with multiple Stone–Wales defects", *Mater. Sci. Eng., A*, 527: 715-723.
20. Yanovsky, Y. G., Nikitina, E. A., Karnet, Y. N., Nikitin, S. M., (2010). "Simulation of deformation and fracture of graphene: effect of size, defects and surface modification", *Phys. Mesomech.*, 13: 329–336.
21. Boukhvalov, D. W., Katsnelson, M. I., (2008). "Chemical Functionalization of Graphene with Defects" *Nano Lett.*, 8: 4373-4379.
22. Shao, Y. Y., Sui, J. H., Yin, G. P., Gao, Y. Z., (2008). "Nitrogen-doped carbon nanostructures and their composites as catalytic materials for proton exchange membrane fuel cell", *Appl. Catal. B*, 79: 89-99.
23. Sumpter, B. G., Meunier, V., Romo-Herrera, J. M., Cruz-Silva, E., Cullen, D. A., Terrones, H., Smith, D. J., Terrones, M., (2007). "Nitrogen-Mediated Carbon Nanotube Growth: Diameter Reduction, Metallicity, Bundle Dispersability, and Bamboo-like Structure Formation", *ACS Nano*, 1: 369-375.
24. Lee, S. U., Belosludov, R.V., Mizuseki, H., Kawazoe, Y., (2009). "Designing Nanogadgetry for Nanoelectronic Devices with Nitrogen-Doped Capped Carbon Nanotubes", *Small*, 5: 1769-1775.
25. Jang, J. W., Lee, C. E., Lyu, S. C., Lee, T. J, Lee, C. J, (2004). "Structural study of nitrogen-doping effects in bamboo-shaped multiwalled carbon nanotubes", *Appl. Phys. Lett.*, 84: 2877-2879.
26. Panchakarla, L. S., Govindaraj, A., Rao, C. N. R., (2007). "Nitrogen- and Boron-Doped Double-Walled Carbon Nanotubes" *ACS Nano*, 1: 494-500.
27. Mortazavi, B. and Ahzi, S., (2012). "Molecular dynamics study on the thermal conductivity and mechanical properties of boron doped graphene." *Solid State Communications*, 152(15): 1503-1507.

28. Mortazavi, B., Ahzi, S., Toniazzo, V., Rémond, Y., (2012). "Nitrogen doping and vacancy effects on the mechanical properties of graphene: A molecular dynamics study" *Phys. Lett. A*, 378: 1146-1153.
29. Mahmood, J., Lee, E.K., Jung, M., Shin, D., Jeon, I.Y., Jung, S.M., Choi, H.J., Seo, J.M., Bae, S.Y., Sohn, S.D. and Park, N., (2015). "Nitrogenated holey two-dimensional structures" *Nature communications*, 6: 6486.
30. Yu, H.L., Jiang, X.F., Cai, M.Q., Feng, J.F., Chen, X.S., Yang, X.F. and Liu, Y.S., (2017). "Electronic and magnetic properties of zigzag C2N-h2D nanoribbons: Edge and width effects" *Chemical Physics Letters*, 685: 363-370.
31. Guan, Z., Lian, C.S., Hu, S., Ni, S., Li, J. and Duan, W., (2017). "Tunable structural, electronic, and optical properties of layered two-dimensional C2N and MoS2 van der waals heterostructure as photovoltaic material" *The Journal of Physical Chemistry C*, 121(6): 3654-3660.
32. Zhang, R., Li, B. and Yang, J., (2015). "Effects of stacking order, layer number and external electric field on electronic structures of few-layer C 2 N-h 2D" *Nanoscale*, 7(33): 14062-14070.
33. Yang, Y., Guo, M., Zhang, G. and Li, W., (2017). "Tuning the electronic and magnetic properties of porous graphene-like carbon nitride through 3d transition-metal doping", *Carbon*, 117: 120-125.
34. Tersoff, J., (1988). "New empirical approach for the structure and energy of covalent systems", *Phys. Rev. B.*, 37: 6991.
35. Tersoff, J., (1989). "Modeling solid-state chemistry: Interatomic potentials for multicomponent systems", *Phys. Rev. B*, 39: 5566.
36. Kinaci, A., Haskins, J. B., Sevik, C., Cagin, T., (2012). "Thermal conductivity of BN-C nanostructures", *Phys. Rev. B*, 86: 115410.
37. Plimpton, S. J., (1995). "Fast Parallel Algorithms for Short-Range Molecular Dynamics", *J Comp phys*, 117: 1-19.
38. Hoover, W. G., (1985). "Canonical dynamics: Equilibrium phase-space distributions" *Physical Review A*: 31: 1695.
39. Allen, M.P., Tildesley, D.J., (1986). "Comput. Simulation Liquids", New York,.
40. Ansari, R., Rouhi, S., Ajori, S., (2013). "Elastic properties and large deformation of two-dimensional silicene nanosheets using molecular dynamics", *Superlattices Microstruct.*, 65: 64-70.